Mechanical properties of wet granular materials

2005 J. Phys.: Condens. Matter 17 S477

(http://iopscience.iop.org/0953-8984/17/9/013)

INSTITUTE OF PHYSICS PUBLISHING JOURNAL OF PHYSICS: CONDENSED MATTER

J. Phys.: Condens. Matter **17** (2005) S477–S502 doi:10.1088/0953-8984/17/9/013

Mechanical properties of wet granular materials

Z Fournier, D Geromichalos, S Herminghaus, M M Kohonen, F Mugele, M Scheel, M Schulz, B Schulz, Ch Schier, R Seemann and A Skudelny

Applied Physics Laboratory, Ulm University, D-89069 Ulm, Germany
and
Max-Planck-Institute for Dynamics and Self-Organization, Bunsenstrasse 10, 37073 Göttingen, Germany

Received 24 November 2004
Published 18 February 2005
Online at stacks.iop.org/JPhysCM/17/S477

Abstract

We elaborate on the impact of liquids upon the mechanical properties of granular materials. We find that most of the experimental and simulation results may be accounted for by a simple model assuming frictionless, spherical grains, with a hysteretic attractive interaction between neighbouring grains due to capillary forces.

(Some figures in this article are in colour only in the electronic version)

Dry sand may be viewed as a fluid phase, given the ease with which it gently runs through the orifice of an hour glass, or forms dunes under the influence of wind—like waves on the ocean. This quasi-fluidity is due to the fact that there is virtually no attractive force between its constituents, i.e., the individual grains. The van der Waals and gravitational interaction energies are very small compared to typical centre-of-mass kinetic energies. Another particularity is the non-equilibrium character of granulates. If one converts kinetic energy to temperature via division by Boltzmann's constant, one finds that the granular motion of even gently shaken sand corresponds to temperatures in the terakelvin range. The obvious fact that even vigorously shaken granulates remain largely at room temperature is due to the vast number of atomic degrees of freedom of the grains, compared to which their centre of mass degrees of freedom are relatively few. The dissipative nature of the intergranular collisions intimately couples the terakelvin heat bath of the granular motion to the atomic degrees of freedom within the grains, which are at room temperature. This extreme non-equilibrium situation is the basis of the striking properties of dry granular matter, which is currently a topic of enormous scientific interest and has seen significant advances in the recent past [1–11].

However, upon adding even minute amounts of liquid, the mechanical properties of the granulate change dramatically. One generally observes a stiffening, a transformation from a more or less fluid state to a somewhat pasty material. This behaviour is well known from everyday life, and is used e.g. in the construction of sand castles. Although it is rather obvious that the formation of liquid capillary bridges between the grains [12–17] plays an important

role here, there is no satisfactory theory for the mechanical properties of wet granulates [5, 16–22]. One of the simpler questions to be asked is whether the capillary force itself yields the stiffer behaviour, or just increases the friction between the grains by pushing them harder together (see below). More complex questions concern the connectivity of the capillary bridge network, and the transformations of the latter upon shearing the granulate. Finally, there are phenomena like soil liquefaction, i.e., the spontaneous transition of a wet granulate from a 'solid' to a viscoplastic liquid state under external shear, which may result in devastating land slides. The dominant physical mechanisms underlying dynamical transitions like this are currently unclear.

1. Wetting granular matter

It appears logical to start with investigating how the granulate acquires the liquid, i.e., the process of penetration of liquid into the granular material. When a dry granulate and a liquid wetting the latter are being brought into contact, the liquid is soaked into the granular pile by means of capillary forces. This process is commonly called spontaneous imbibition, and one might justly ask to what extent the structure of the imbibition front determines, or influences, the final distribution of liquid within the granulate. The process of imbibition of a liquid into a random medium also plays a key role in many other problems of general interest, such as oil recovery, or irrigation in agriculture.

Inspired by this tremendous practical importance, there has been a lot of theoretical work trying to predict the structure of the advancing liquid front. While earlier models based on percolation ideas were rather crude, there has been considerable improvement in recent years, as nonlocal effects were explicitly included in the dynamics [23–26]. These come about from lateral pressure gradients close to the front line, and should strongly affect the statistics of the dynamical front roughness. It has been predicted that there be a crossover from a large roughness exponent at short length scales (non-local regime) to a smaller, universal roughness exponent at larger scales (local regime). The latter regime is, for small excursions, expected to be described by the well known Kardar–Parisi–Zhang (KPZ) equation [27]. However, since most of the theories are merely based on scaling arguments, it was not clear at which length this crossover takes place. In the case of imbibition into a granulate, it is not only of interest whether this crossover length exists at all, but if so, whether it is smaller or larger than the diameter of the grains. Only in the latter case may one expect nonlocal effects to be of significance for the distribution of liquid in the pile.

Recent experiments on capillary ascension between roughened glass plates have shown for the first time that the crossover length really exists [28, 29]. The main advantage of these experiments was that the separation of the glass plates provided an extra tuning parameter which could be systematically varied. Theory predicts that the crossover length varies as the square root of the plate distance. It was found that this was indeed the case, corroborating the theoretical prediction. A granular material, which consists of grains in mutual contact, corresponds thus to a plate distance comparable to the amplitude of the roughness, which was a few microns. Extrapolating the crossover length to this situation, one obtains only a few hundred microns, which is comparable to the typical size of the grains in a granulate. We can thus conclude that, at least in generic cases of imbibition into a granular material, the imbibition front follows KPZ scaling. Quite generally, in porous media like sandstone or a granular pile, the scale for pressure variations along the imbibition front is set by the size of the voids. For the granulate, this is of order $\Delta p \approx \gamma/R$, where γ is the surface tension of the liquid, and R is a typical radius of the grains. Any structure of the imbibition front on larger scale will be connected to pressure differences small as compared to γ/R, and thus not be capable

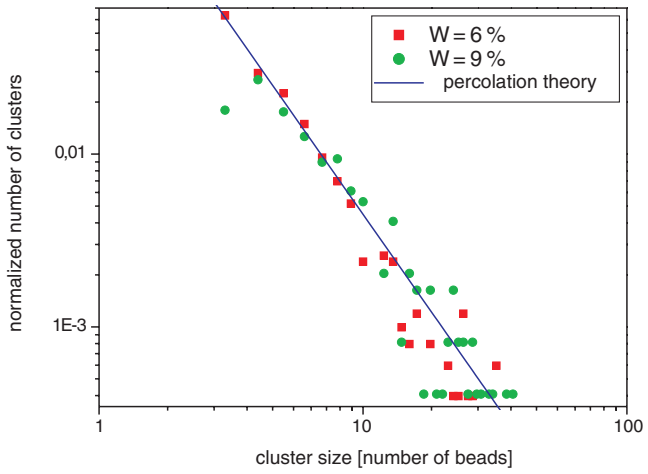

Figure 1. The relative frequency of clusters of different size, formed by liquid clusters of paraffin gluing several glass beads together. If the liquid paraffin is distributed statistically within the pile, one would expect the cluster sizes to be distributed according to the bond percolation model. This is represented by the solid line, and agrees quite satisfactorily with our data.

of overcoming pinning effects on the scale of the grain size, or considerably affect the flow behind the front. As a general result, we can conclude that non-local effects can be considered negligible on all length scales large compared to the typical grain size. Other mechanisms such as air entrainment will be more important in shaping the final structure of the front.

Imbibition leads to a state of the granulate in which part of it is still dry, while the other is well saturated with liquid. In order to prepare what may be justly called a wet granulate, i.e., a ternary system consisting of grains, water and air, all evenly distributed within the sample, one has to agitate the material in some way. The imbibition front is then broken up into a number of fronts, and the question remains of to what extent the final distribution of liquid inherits some features of the KPZ scaling of the single imbibition front. One might anticipate that these will be hard to detect, if present at all, but this remains to be tested experimentally.

We have therefore prepared samples of spherical (1.8 mm diameter) glass beads as the grains, wetted by liquid paraffin at 100 °C [29]. The volume fraction of the paraffin was 6% and 9%, respectively. As will be shown below, this is in the range where liquid bridges start to form wet clusters. The samples (volume about 100 ml) were agitated until the liquid appeared evenly distributed. Upon cooling down to room temperature, the paraffin solidified, forming clusters of beads by gluing them together. Upon gentle shaking, it was possible to separate these clusters and to count them according to their size. For a random distribution of liquid, the bond percolation model predicts that the number of clusters $n_c(s)$ of size s scales as $n_c \propto s^{\tau}$, with $\tau = 2.18$ [30]. As figure 1 shows, this is well fulfilled for both volume fractions examined. So far our findings are consistent with the liquid being well randomized within the granulate, without inheriting structural features from imbibition front dynamics. To gain deeper insight, however, it would be desirable to directly observe the shape of the liquid/gas interface forming in the pile. This will be described in the next section.

2. The network of capillary bridges

At small liquid content and after sufficient equilibration, the interior of the wet granulate is expected to be characterized by a network of liquid bridges connecting adjacent grains in

contact. These bridges should be shaped as minimal surfaces, each having the same mean curvature. It is clear that the connectivity of this network of liquid bridges is of importance for the mechanics of the wet granulate [12, 18, 21, 31], be it directly due to the capillary force itself or to the enhancement of the mutual friction between the grains due to the increased internal pressure. This depends upon the packing geometry of the pile, which is an interesting and complex topic in itself. Even for the random close packing of spheres, which is the 'simplest' random packing and has been much studied in the past [32, 33], the coordination and nearest-neighbour relations are still under investigation [34]. We therefore performed experiments in order to find relations between spherical packing geometries, nearest-neighbour coordinations, and the capillary bridge network.

In order to observe and count the single bridges we used an index matching technique [35]. We used glass beads with mean diameters of 375 μm or 555 μm. The diameters were slightly polydisperse (several % width of distribution) in order to avoid crystallization. Their refractive index was 1.51. The air in the sample was replaced by a mixture of toluene and diiodomethane which was adjusted to the same refractive index as the glass beads (11.9% diiodomethane). The fact that the samples were still not completely transparent was due to some variations in the refractive index of the glass beads. However, it was quite possible to zoom through the pile with a long distance optical microscope. In this way, individual bridges, their network, as well as liquid clusters as remnants of the imbibition process could be observed and investigated. As the wetting liquid, we added small amounts of water, with some fluorescein dissolved to ease observation. The aqueous phase wets the glass beads in the presence of the index matching liquid and forms capillary bridges, which may be directly observed.

The granulate was put into a commercially available cuvette (0.95 cm $\times$ 0.95 cm $\times$ 4 cm, filling height: 2.5–3 cm) filled with the toluene–diiodomethane mixture. After the wetting liquid was added, the cuvette was sealed, tilted by 90°, and shaken. The shaking motion consisted of small horizontal circles with an amplitude of 5 mm and with a frequency of roughly 30 Hz, and was applied for a few minutes, until the liquid appeared evenly distributed. The homogeneity of the distribution could be judged by inspection of the fluorescence under an ultraviolet lamp. After shaking, the volume fraction of the glass beads was $\rho \approx 0.57$, as determined by direct observation and counting of beads. We thus found the wet granulate packed significantly less densely than the loose random packing of $\rho_{\mathrm{lrp}} = 0.60$ observed for the dry case [32]. Measurements made immediately after this preparation will be referred to as random loose packing measurements.

By gently tapping against the sample after shaking was terminated, we could reach a random packing density of $\rho \approx 0.62$, which is closer to the volume fraction of random close packing ($0.64 =: \rho_{\mathrm{rcp}}$ [32]). Measurements made subsequently will be called random dense packing measurements. It should be mentioned that we did not observe a measurable dependence of packing densities upon the amount of wetting liquid added. An obvious reason is that the forces exerted by the bridges are largely independent of bridge volume [15, 36].

In what follows, we report measurements of the average number of capillary bridges per glass bead, as found by direct inspection with a optical microscope. We define the water content W as the volume of (aqueous) liquid divided by the total sample volume. When only very small amounts of liquid were added, there was no formation of capillary bridges. This is because the liquid was first trapped on the surface due to the bead roughness [14, 15, 36], as can be seen in figure 2(a). Only at a water content of $W_{\mathrm{b}} := 0.07\%$ were bridges on almost every bead contact formed (see below). Figure 2(b) illustrates the case for fully developed bridges.

The connection between the roughness amplitude δ and the saturation bridge volume is given by $w_{\mathrm{b}} \approx 2R\delta^2$, where R is the bead radius, and w_{b} the volume of a bridge at the water

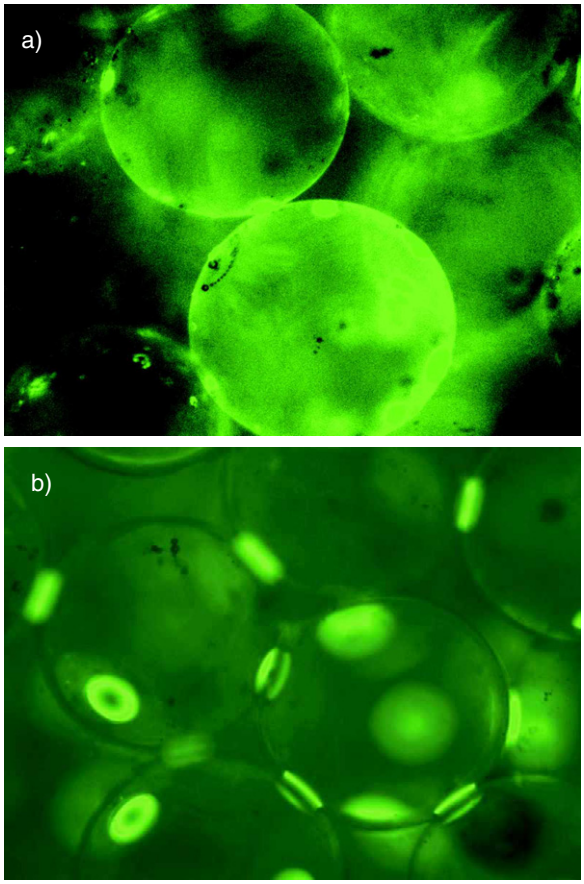

Figure 2. Fluorescence microscope images for different water contents W, with glass beads of diameter 375 μm. (a) $W = 0.055\%$; no bridges have formed yet. All liquid resides within the roughness of the glass surface. (b) $W = 0.2\%$; capillary bridges between the beads have formed. The sensitivity of the camera is correspondingly reduced, such that the liquid trapped in the roughness of the glass surface is no longer visible.

content of saturation, W_b [14]. Our measurements suggest that the relationship between the water content W and the volume of a single bridge w is generally given by $w = \alpha R^3 W$, where $\alpha \approx 0.25$ [18, 37]. From $W_b \approx 0.07\%$ we get $\delta \sim 500$ nm, which is similar to the peak-to-peak roughness we found from the inspection of the beads by atomic force microscopy.

The average number of bridges per bead was obtained by zooming with the microscope through the sample and counting the bridges. This was carried out at variable liquid content for random loose packing ($\rho = 0.57$) as well as for random dense packing ($\rho = 0.62$). The dependence of N on the water content is shown in figure 3. At a water content slightly smaller than W_b it rises sharply, then levels off around $N \approx 6$. It can be seen that $N(W)$ for the random dense packing is about 10% larger than $N(W)$ for the random loose packing. W_b is the water content at which a capillary bridge exists if (and only if) two beads touch, i.e. if their surface distance d is zero. The non-zero values at $W < W_b$ are due to inhomogeneities of the glass surface properties. For $W > W_b$, one expects roughly as many bridges per bead as there are close contacts ($d = 0$).

It is instructive to compare our results to the so-called caging model [34]. This assumes a random packing structure of spheres defined by the condition that each sphere experiences just enough close contacts to fix its position in space. For the average number of close contacts, N_c, recent investigations of this model yield $N_c = 4.79$ for a random packing of equally sized (monodisperse) spheres [34]. For a liquid content only slightly above W_b, N should be close

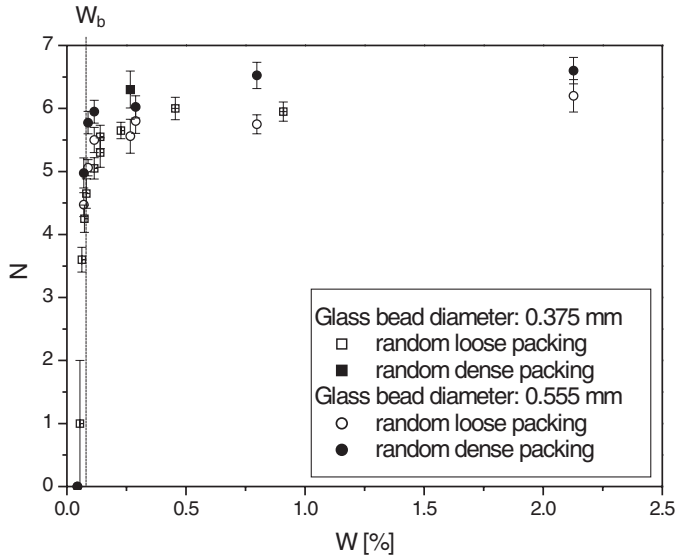

Figure 3. Average number of capillary bridges $N(W)$ as a function of the water content W. Error bars are standard deviations.

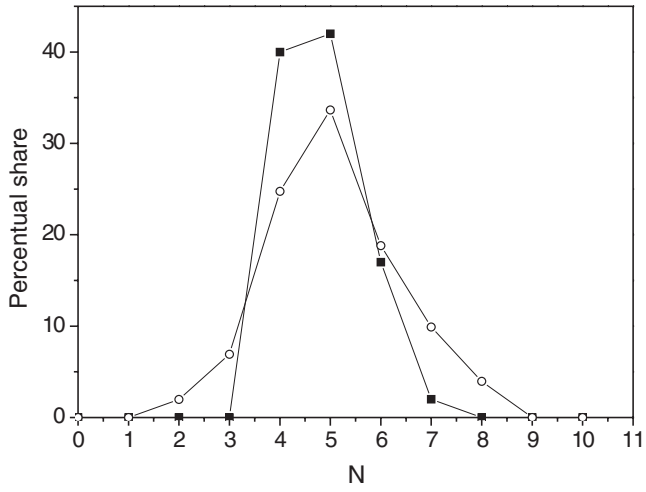

Figure 4. Distribution of the number of bridges per sphere. Our measurements are represented as open symbols, obtained with random loose packing at $W = 0.15\%$. Closed symbols correspond to simulations [34].

to N_c. Figure 4 shows that this is indeed the case. The centres of the distributions are quite well aligned, although the width of the experimental data is significantly larger. We attribute this to the polydispersity of our sample. If W is well above W_b, $N(W)$ should be larger than N_c, because liquid bridges may exist even between surfaces which have a small but finite distance from each other. At every collision between two beads, i.e. at a bead surface distance $d = 0$, a new bridge forms. After impact, a 'stretched' bridge emerges, suspended between the neighbouring beads. Consequently, for $W > W_b$ there should be more bridges than bead contacts.

More precisely, every bridge will survive until the surfaces of the beads carrying it separate farther than a certain critical distance, $d_r(W)$, at which the bridge ruptures. Let us thus consider the average number of spheres, $N_r(W)$, which have a surface distance of d_r or less to the sphere under investigation. It is clear that for the number of capillary bridges we have $N_c \leqslant N(W) \leqslant N_r$. Since on average there will be half of the surfaces approaching, and

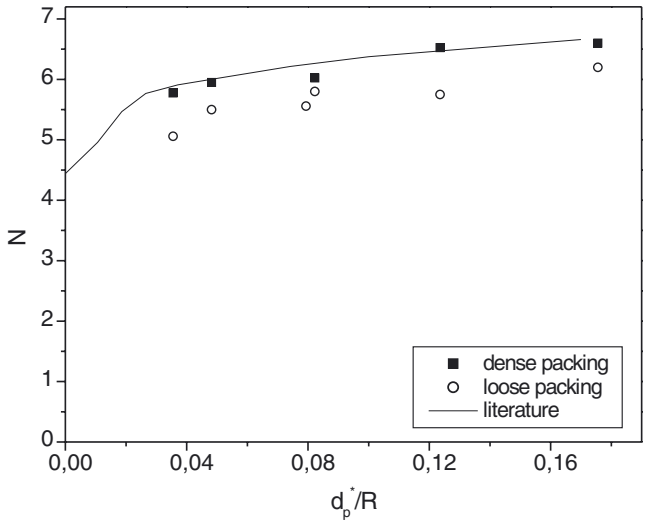

Figure 5. The average number of bridges per sphere, as a function of the normalized critical distance, d_r/R. The solid curve represents the number of spheres within a certain distance, as obtained numerically from the caging model.

half departing from each other, one might be tempted to set $N(W) = (N_c + N_r)/2$. However, the correct result for N is less than this because approaching surfaces may miss each other and never touch, thus never forming a bridge. This depends on the impact parameter of the relative motion of the neighbouring spheres. Integrating over all possible impact parameters, one readily finds $N(W) = N_c + (N_r(W) - N_c)/\beta$, with $\beta \approx 1.45\frac{d_r}{R} + 2$. Since $d_r \ll R$ in most experimentally relevant cases, $\beta = 2$ is a reasonable approximation, returning to the rough estimate above.

Since data of $N_r(d_r)$ are available for the caging model [33, 34], we can directly compare our experimental results with this model on the basis of the relation derived above. Figure 5 shows our measured $N(W)$, plotted versus the rupture distance $d_r(W)$. The latter was calculated from the relation [36]

$$d_r = w^{\frac{1}{3}} + \frac{1}{10}\frac{w^{\frac{2}{3}}}{R}.$$

In this case, the data were obtained with 555 μm diameter beads for random loose packing as well as random dense packing. These beads were used since the polydispersity was comparably small (a few per cent), such that comparison with the theoretical data (obtained for monodisperse systems) appeared sensible. Differences in packing density are expected to show up in the number of close contacts. We thus allowed for vertical adjustment of the theoretical curve, such that $N_r(0) = N(W \approx W_b) = N_c$. The solid curve represents values of N for dense packing which were calculated from literature values of N_r [33], using $N_c = 4.4$. The agreement with our measurements for random dense packing (squares) is quite satisfactory. For random loose packing (circles), good agreement is obtained for $N_c = 3.3$.

The values for N_c as thus obtained from our measurements differ from the value $N_c = 4.79$ of the caging model. The latter is in agreement with the experimental measurements of the number of close contacts for random close packing ($\rho = 0.64$) [33]. It is interesting to note that our measurements suggest a linear relationship between the differences $4.79 - N_c$ and $0.64 - \rho$, as shown in figure 6. In particular, we find $4.79 - N_c \approx (20.5 \pm 1.5)(0.64 - \rho)$.

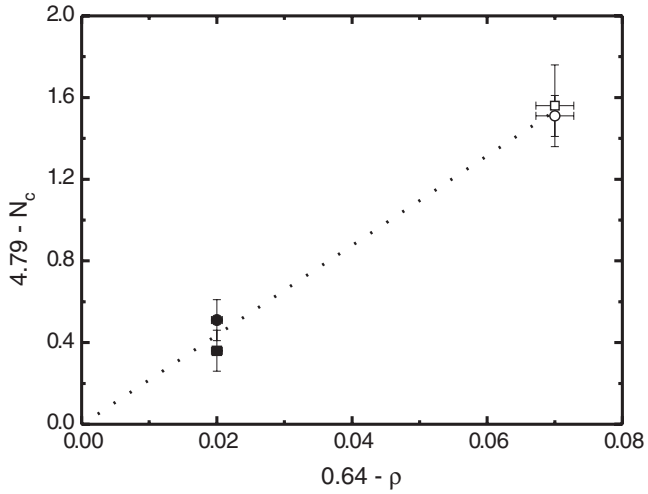

Figure 6. Relation between the packing density and the average number of close contacts, as inferred from the average number of capillary bridges.

It may be left to further studies whether this relationship is a universal property of random sphere packings.

3. Shearing wet granular matter

After having elaborated on morphological aspects of the distribution of liquid within a wet granulate, let us now turn to mechanical properties and their possible relation to these liquid morphologies. The most straightforward question to pose concerns the shear rigidity of the material, i.e., what shear stress is necessary in order to sustain a certain shear rate. The main experimental problem here is the occurrence of avalanches and arching, which make it difficult to establish a shear rate which is homogeneous over the whole sample. This is particularly annoying in experiments concerning the critical angle of granular piles [17, 22], but also plays a role in experiments in which the granulate is sheared by the motion of rigid boundaries [5, 6, 8].

In order to avoid such avalanches in our experiments we have sheared granular matter in a comparably well defined, homogeneous way. Figure 7 shows our experimental set-up. We filled the granular material (spherical glass beads as above) into a cylindrical cell made of Plexiglass with a diameter of 2 cm and a length of 1 cm. The flat sides of the cell each consisted of a thin latex membrane, with a thickness of 300 μm. Adjacent to each membrane was a cylindrical chamber filled with water, and connected with a thin metal pipe to a syringe. The pistons of the syringes were connected to spindles which could be moved with computer-controlled stepper motors. When the two pistons were moved at equal speed but in opposite direction, the sample between the membranes was deformed at constant volume and well defined speed. The tension of the membranes ensured a roughly parabolic deformation, and thus a flow profile similar to Poiseuille flow within the sample. In this way, avalanching and arching can be kept to a tolerable minimum, and a rather homogeneous shear deformation of the sample as a whole is achieved. Piezoresistive sensors were used to record the pressure in both chambers.

The granulate was filled through a sealable orifice in the top of the cell. A density corresponding roughly to that of random dense packing, $\varepsilon = 0.63$ [32], was achieved by tapping against the cell. As the wetting liquid we added well defined amounts of water to the granulate by means of a micropipette. After sealing the cell, the sample was sheared back and

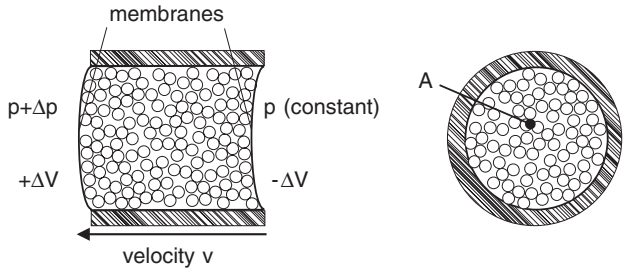

Figure 7. Experimental set-up. The granulate is sheared with a mean velocity v by a shearing volume ΔV. The pressure difference Δp is recorded. A is the cross-sectional area. The left drawing displays a slice of the shearing cell viewed from the side and the right a slice of the cell viewed from the front, respectively.

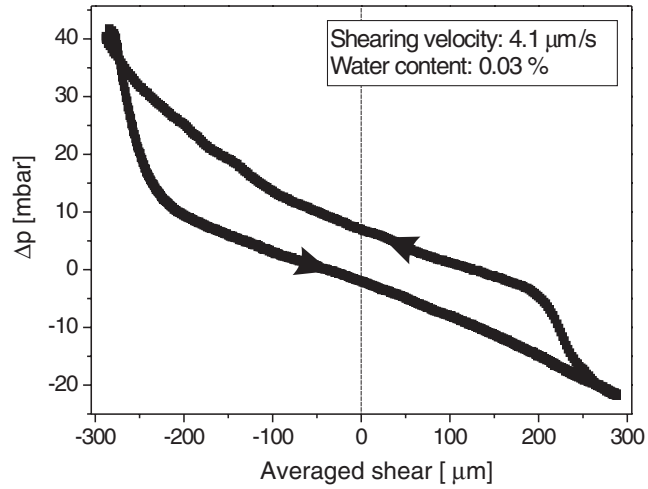

Figure 8. Differential pressure curve of a sheared granulate. The hysteresis is clearly visible (the curve is passed anticlockwise).

forth in the manner described above in order to evenly distribute the water. After about one half hour of repeated shearing, the pressures in the chambers had become reproducible (the same pressure curve in each cycle), and the measurement was started.

At the beginning of the measurement, the absolute pressure was adjusted. Then the sample was sheared back and forth with a constant velocity of the motors. The mean shear rate v in the sample is $v := \frac{\Delta V}{tA}$, where $\Delta V/t$ is the rate of the change of the volume of each reservoir, and A is the area of the membranes. During these motions the differential and the absolute pressure, the motor positions and the time were continuously recorded. The control parameters were the liquid content W, the shearing velocity v and the absolute pressure p.

Figure 8 shows a typical differential pressure curve, plotted versus the (spatially averaged) shear $\frac{\Delta V}{A}$. The main features are the slope of the curves and the strong hysteresis. The slope of the two branches corresponds to the restoring force exerted by the rubber membranes. The reason for the hysteresis is the yield stress of the granulate which opposes the applied shear with a certain pressure. In other words, the vertical width of the hysteresis loop corresponds to the shear stress which, if applied to the granulate under investigation, would cause the latter to yield at a shear rate equal to that applied in the experiment. In order to determine the

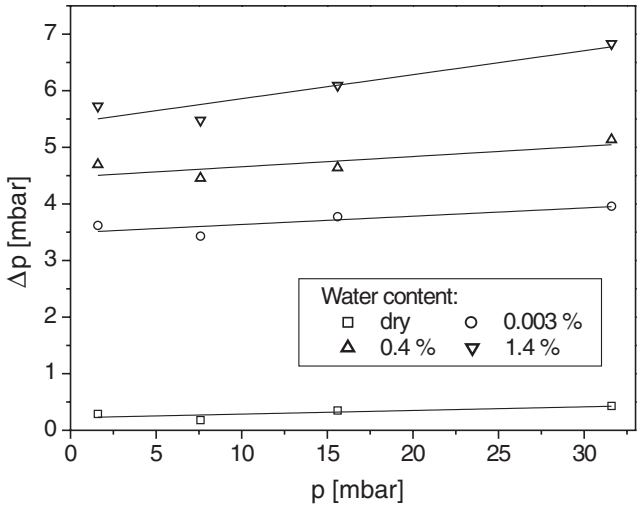

Figure 9. Dependence of the differential pressure Δp on the absolute pressure p for $v = 16.5\ \mu\mathrm{m\ s}^{-1}$.

(rate dependent) yield stress of the sample, we took the difference between the upper and the lower branch of the hysteresis curve at zero shear (dashed line), and divided it by two. We have chosen the total shear to be large enough to overcome the elastic regime of the granulate, i.e. the shear was big enough to enable irreversible particle motions [38].

Our set-up enables us to answer a number of important questions. First of all, as mentioned above, it is not clear by which mechanism the capillary bridges enforce the granulate. If it were by increasing the friction forces between the grains, due to the increased normal force between adjacent grain surfaces, we would expect that increasing the external pressure on the membranes would have a similar effect. The internal pressure due to the presence of the capillary bridges can be easily evaluated. For ideal spheres, each bridge exerts a force of $F_\mathrm{B} = 2\pi R\gamma\cos(\theta)$ [36], where R is the radius of the beads, γ is the surface tension of the liquid, and θ is the contact angle of the liquid with the bead material. Roughness can only reduce this force [15], hence we have in general $F_\mathrm{B} \leqslant 2\pi R\gamma\cos(\theta)$. If $N \approx 6$ is the coordination number of the bridge network and ρ its packing density, we readily find $p = \mathrm{d}E/\mathrm{d}V = NF_\mathrm{B}d/3V \leqslant N\rho\gamma/2R \approx 1.9\gamma/R$. For beads with a diameter of 175 μm wetted by water, this yields a pressure of about 8 mbar. This sets the scale for the external pressure to apply. If the yield stress of the pile were provided by mutual friction between the grains, applying 8 mbar externally would be expected to increase the yield stress to a similar extent as did the addition of the liquid.

The dependence of the yield pressure Δp on the absolute (external) pressure p is shown in figure 9. It is clearly seen that raising the external pressure even above 30 mbar does not noticeably change the pressure difference, i.e., the yield pressure of the material. In contrast, the addition of water entails a dramatic change. We see that the effect of the bridges on the yield pressure is much larger than the effect due to increased friction at a pressure corresponding to the internal pressure exerted by the bridges. Hence we can conclude that the increase in yield stress of a wet pile of glass beads, as opposed to the dry one, is mainly due to the topology of the bridge network, not to increased friction. It remains to be investigated whether this also holds for non-spherical grains. But our results show that the bridge network topology is indispensible for explaining the main features of the wet material.

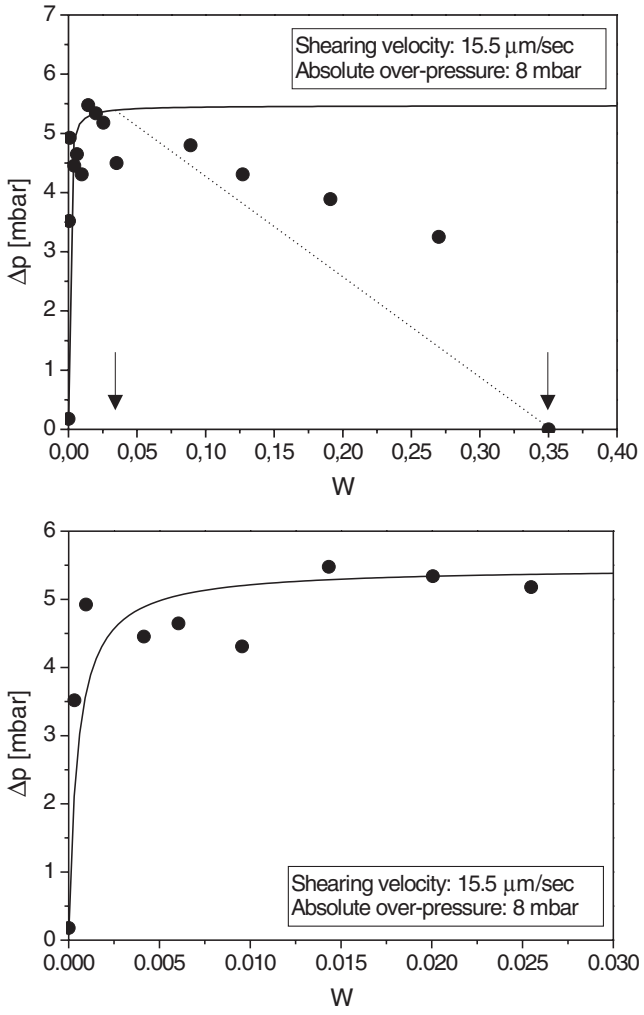

Figure 10. Dependence of the differential pressure Δp on the liquid content W.

In what follows, we define the yield pressure as the pressure difference Δp extrapolated to zero external pressure. Its dependence upon the liquid content, W, is shown in figure 10. The upper and the lower graph both show the same measurement, but the lower graph is 'zoomed' into smaller W in order to display variations at very small water content.

Let us first discuss the latter. We see that the yield stress is close to zero only at very small liquid content, and sharply rises to an almost constant value. This behaviour is directly connected to the capillary bridge force between slightly rough (non-ideal) beads, which can be written as [36] $F_{\mathrm{B}} = 2\pi R\gamma \cos\theta f(w)g(d)$, where $f(w)$ depends upon the roughness of the bead surface. The monotonically decreasing function $g(d)$ describes the dependence of the bridge force upon surface distance, with $g(0) = 1$, and $g(d \geqslant d_{\mathrm{r}}) = 0$. The function $f(w)$ describes effects of surface roughness. For perfect spheres, $f(w) = 1\ \forall w$, but for a rough surface, it tends to zero as $w \to 0$. The shape of $f(w)$ has been discussed in detail before [15], and may be approximated by

$$f(w) = \left[\frac{w}{w + w_{\mathrm{b}}}\right]^{\mu} \tag{1}$$

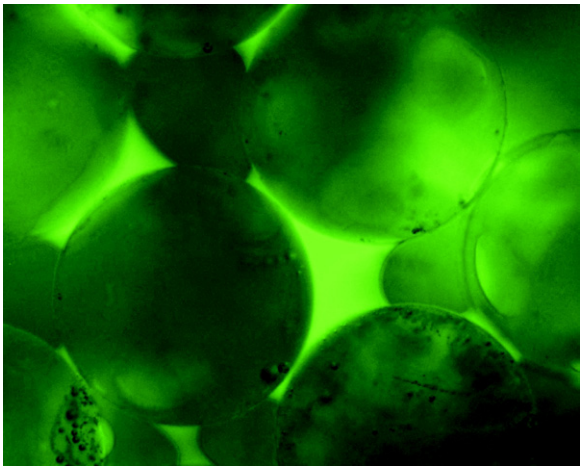

Figure 11. Liquid clusters at higher liquid content ($W \approx 3\%$).

where μ is related to the roughness exponent of the bead surface, χ, via $\mu = (2 - \chi)(2 + \chi)$. For (typical) scratch and dig roughness, χ is close to zero, and $\mu \approx 1$. This corresponds to the regime found by Hornbaker *et al* [14]. In the opposite case, when $\chi \to 1$, we have $\mu \to 1/3$. We see that μ is confined to a narrow interval, and is very probably close to one in our system. In what follows, we will set $\mu = 1$ and discuss the impact of possible deviations from this value where appropriate. We know from AFM measurements that the bead roughness is $\delta \approx 500$ nm (see above). We thus calculated the force of the capillary bridges and plotted it in the graphs in figure 10 as the solid curves, with the saturation height as the only fitting parameter. Within experimental scattering, this describes our data quite well within the range displayed in the lower graph.

As can be seen in the upper graph of figure 10, the granulate became softer for $W \geqslant 4\%$ (left arrow), and could be sheared with nearly no force in the fully saturated case (right arrow). The reason for this behaviour is the formation of liquid clusters in the pile. This occurs at liquid content of $W > 3\%$, and can be well observed by optical microscopy using the index matching technique described above. These clusters have less liquid/gas interfacial energy and thus exert less force to mechanically stabilize the pile. Figure 11 illustrates this for a liquid content of about 3%. After $W \geqslant 4\%$ the number of the clusters decreases again, since many clusters merge due to their increasing size. This tendency continues with increasing W. The percolation threshold [30] is reached at $W \approx 11\%$. If one assumes simplistically that the total cluster volume increases linearly with W and further takes into account that the beads inside such a cluster are not affected by any capillary bridges, one should roughly expect a linear softening. As can be seen in figure 10, this is not the case, which suggests a more complicated mechanism. This may be left to future studies. We just note in passing that above the percolation threshold, i.e., for the data points at $W = 0.19$ and 0.27, experimental scattering in Δp was very large (more than 50%), probably due to the possibility of long distance transport within the percolated liquid structure. It is clear that at full saturation no interface is present and the granulate is as soft as in the dry case.

Let us now turn to the dependence of Δp on the shear rate v. As figure 12 shows, Δp depends strongly on v for the wet, and only for the wet cases. We found no clear dependence of Δp on v for the dry case. This is not surprising, since the applied absolute pressures were quite small. In this case, neither for the free sliding regime [6] nor for the stick–slip regime [7, 8]

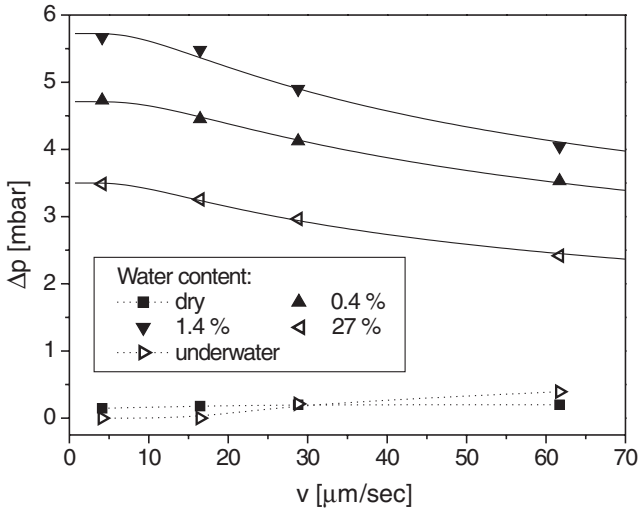

Figure 12. Dependence of the differential pressure Δp on the mean shearing velocity v for an absolute pressure $p = 7.6$ mbar.

is a clear dependence of Δp on v [6] expected. For the underwater case we found a small increase of Δp with v for the higher velocities (see figure 12), which we assume to be due to the viscosity of the surrounding water, which is pressed through the granular matter during shearing.

As mentioned, a dependence of Δp on v was clearly visible for the wet cases alone. Here we found a general decrease of Δp with v. This behaviour can be explained directly in terms of the temporal evolution of the involved liquid capillary bridges. It is well known that the mechanical properties of wet granular matter change with time with the granulate getting stiffer, i.e. there occurs 'ageing' [16]. A main reason for this observation is that the capillary bridges grow with time due to liquid flowing from the particle surfaces into the liquid bridges [37]. From our own measurements we found that

$$w \propto 1 - \mathrm{e}^{-\frac{t}{t_0}}$$

with the bridge volume w and a characteristic time constant t_0 which depends on the liquid and particle properties is of the order of a few minutes [37].

If we now assume that, due to the geometry of the pile, the number of ruptured bridges per shear is constant, we obtain in a straightforward manner

$$\Delta p \propto \left(1 - \mathrm{e}^{-\frac{t}{t_0}}\right)^{\frac{1}{3}} \approx \left(1 - \mathrm{e}^{-\frac{1}{t_0 v_\mathrm{s}}}\right)^{\frac{1}{3}}$$

with v_s being the shear rate. As can be seen in figure 12 (three upper curves), the measurements are in accordance with the fit curves. The values for t_0 as obtained from the fits were about 5 min. This is similar to the time constant we have measured independently by optical inspection of individual liquid bridges [37].

A main conclusion from these observations is that the formation dynamics of the liquid bridges can alone account for shear thinning effects. This is in contrast to a widespread opinion that dilation effects are the main reason for shear thinning. This is particularly interesting because shear thinning is a major requirement for avalanching to occur, as observed in landslides. We will come back to this point below.

4. Dynamic phase transitions

Now that we have elaborated on an appropriate microscopic picture of wet granulates, we might try to tackle some of the more complex dynamic topics. We have seen that some hallmark features of wet granular materials can be well understood with rather simple concepts. It thus appears reasonable to try to understand the basic mechanisms of complex phenomena such as soil liquefaction in a similar way. More precisely, we will take the microscopic picture developed above and use it to find again the least complicated model which accounts for the main features observed. We will hereby focus on dynamical phase transition phenomena, such as fluidization and soil liquefaction.

5. The role of hysteretic interaction forces: wet granulates in-silico

The previous section suggests that it is the network of the capillary forces itself which yields the stiffness of the wet granulate, as opposed to the dry one. The most striking feature of the interaction by capillary forces is the hysteretic nature of that force. Two grains (or beads) must touch each other for a bridge to form. However, once it has formed, it will survive a significant distance of separation of the bead surfaces, until it finally ruptures at a finite distance. Note that there is no qualitative difference in the behaviour of wet sand and wet glass beads, which suggests that the pointed shape of natural grains is not essential for the main features, although it surely changes some characteristics quantitatively. Thus our main hypothesis is that the hysteretic nature of the interaction is sufficient for explaining the main mechanical features, both static and dynamic, of a wet granulate.

In order to test this hypothesis, we must prepare a granulate which has no other interactions than the hysteretic force. This cannot be done experimentally, since all real beads exhibit friction, but it can be done on a computer. The system we have investigated consists of a few hundred spheres which experience only nearest neighbour central forces, i.e., there is no friction between adjacent surfaces. The spheres were chosen slightly polydisperse in order to avoid spurious crystallization effects. The density was chosen close to random close packing. The system was placed in a cubic box with periodic boundary conditions in all three dimensions. Newton's equation of motion has been solved using a Runge–Kutta algorithm. The program was written in FORTRAN and could be implemented on parallel processors in a straightforward manner, but could as well be run on a PC.

First of all, there must be repulsive forces modelling the hard core interaction of the grains. We have tried several repulsive potentials. The steepest one was an 'exact' hard core, in which accidental overlaps were removed by back tracing. The softest one was a r^{-12} central potential; higher exponents were also used. The most important point is that our findings were independent of the repulsive potential we used. For the attractive force contribution modelling the capillary bridges, we chose a non-conservative, hysteretic interaction. To the force derived from the repulsive contribution, we added a constant attractive force of unit strength between all pairs of particles which were withdrawing after an impact. This force, which corresponds to the 'stretched bridges' discussed above, was switched off as soon as the separation distance, d, had reached a certain critical value, d_{r}. It should be well noted that this models capillary bridges that form instantaneously, which may be considered a gross simplification. We will return to this point below.

A shear field was applied to the whole system, resembling a gravitational field with oscillatory spatial variation. More precisely, the acceleration of gravity was chosen to be $\vec{e}_z F \cos(2\pi x/L)$, where L is the lateral dimension of the box. There was thus a shear field within the granulate, while the total force on the system was close to zero. Simulations were run

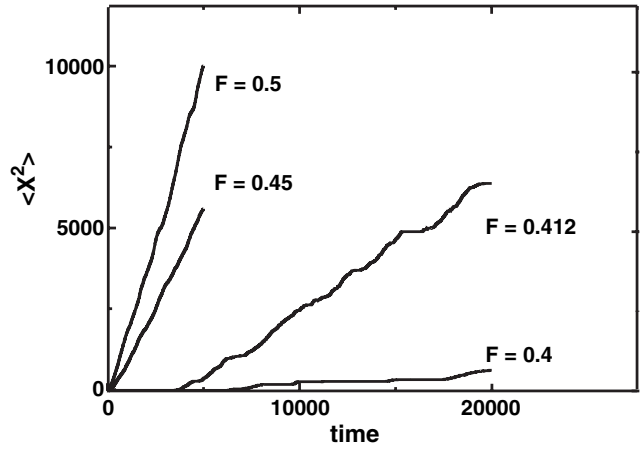

Figure 13. The mean square displacement of the spheres in our simulation of a granular pile under external shear stress. For larger values of F, an almost perfectly linear behaviour is found, indicative of diffusive transport.

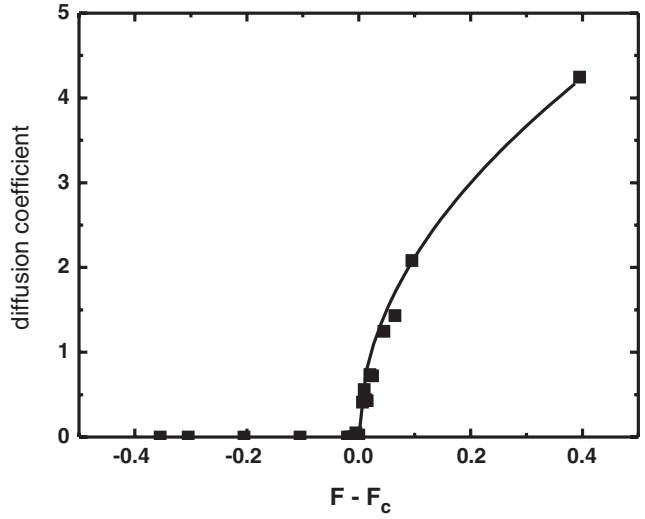

Figure 14. The ensemble averaged diffusion coefficient of a simulated pile of spheres. The solid curve represents the form $D = D_0(F - F_c)^{1/2}$.

at different values of F, and the motions of the spheres were recorded. It proved particularly instructive to plot the mean square displacement of the spheres as a function of simulation time. As it is shown in figure 13, we found roughly straight lines for values of F well above 0.4. This points to a diffusive behaviour, and we thus can, at least in this regime, characterize the motion by a diffusion constant, $D := \mathrm{d}\langle X^2\rangle/\mathrm{d}t$. Well below $F = 0.4$, only small scale motion was present. As long as there are no topological transformations in the neighbourhood relations, no bridges are broken, and the system is Hamiltonian. Thus there is a small scale Brownian-like motion which persists throughout the simulation time by energy conservation.

When the diffusion coefficient D is plotted as a function of the applied shear force F, critical behaviour becomes obvious. As figure 14 shows, there is almost no diffusive motion

below a critical force of about $F_c \approx 0.42$. Close to this critical force, we found strong avalanching effects within the system, and the average energy of this avalanching diverged algebraically at $F = F_c$ [39], but diffusive transport remained slow. Above F_c, the latter builds up sharply, as can be seen from the figure. This behaviour is well resemblant of phenomena like soil liquefaction or land slides, where a wet granulate suddenly becomes fluid under the influence of external shear. For $F \geqslant F_c$, our data can be well fitted with a critical exponent of 0.5, as indicated by the solid curve.

It is interesting to compare the behaviour displayed in figure 14 with the shear thinning effects shown in figure 12. Identifying the rate of diffusion with the shear rate and the applied pressure difference with the applied shear force, we observe that there is no shear thinning in the simulation results. In contrast, larger relative motion of the particles (i.e., larger D) corresponds to larger applied stress, F. Although this is at first glance a qualitative discrepancy, it is straightforward to see where it comes from. The shear thinning observed in the experiment was argued to be due to the finite formation time of the liquid bridges. But in the simulation, they form instantaneously, so this effect must be absent here. Consequently, what we see in the experiment and in the simulation is precisely what we expect if our model assumptions are true.

Furthermore, from our considerations of the bridge network, as illustrated in figure 3, we see that the number of bridges per bead is a rather robustly constant quantity. From figure 6, we find that the percentage change in coordination number is about 2.7 times the percentage change in density. We found that the yield pressure drops upon shear by up to 30% in our experiments. Hence if this were due to dilatancy as the most important mechanism, we would have to assume a drop in density by shear of some $30/2.7 \approx 11\%$. This is more than has ever been observed in dilatancy experiments. We thus conclude that shear thinning in wet granulates, at least in the range of parameters investigated here, is due to the dynamics of capillary bridge formation, rather than due to dilatancy.

Coming back to the critical exponent of the diffusion constant, let us briefly outline a microscopic picture which may explain its value of 0.5. The distance a sphere traverses during a site exchange process scales with the sphere radius, R. The energy the sphere takes up from the applied shear field during that process is thus of order R^2F/L. At the same time, a certain number, G, of capillary bridges must be broken. G is a geometrical factor of order unity which depends upon the packing density. The total energy which must be afforded to break these bridges is thus Gd_rF_B, where F_B is the bridge force. The energy which is left, and afterwards randomized into disordered motion by subsequent impacts, is thus $T := R^2F/L - Gd_rF_B$. The diffusion constant is equal to the average jumping distance, times the particle velocity. The latter is given by $\sqrt{2T/m}$, where T is the kinetic energy. If we identify this with the randomized energy above, we have immediately

$$D = D_0 (F - F_c)^{1/2} \tag{2}$$

with $F_c = Gd_rF_BL/R^2$. The critical exponent of $1/2$ is indeed consistent with our simulation results. The critical force is thus predicted to scale proportionally to the rupture distance, d_r. In figure 15, it can be seen that this is at least qualitatively the case. In fact, it is expected to scale sub-linearly (as observed), since the number of bridges broken upon site exchange will decrease with increasing d_r. In our simulations, d_rL/R^2 was of order one, such that $G \approx 2$ would explain our data, which is not far from what might be expected.

Our simulations thus corroborate the idea that our simple picture of capillary bridges may well account for the main features observed in a wet granulate. We can even provide a mean field argument which accounts for the critical exponent we found in the simulation. In what follows, we return to the laboratory experiment, and try to understand our findings by means of the simple model outlined so far.

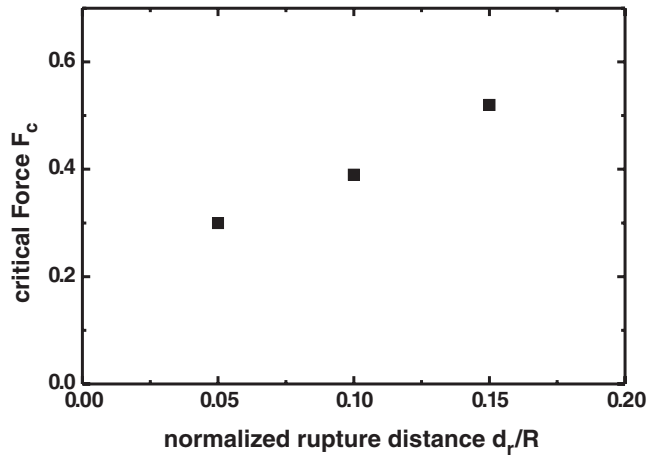

Figure 15. The normalized critical force, F_c/F_B, versus the normalized rupture distance, d_r/R.

6. Horizontal agitation: fluidization by energy

Some experiments have been done before on the influence of liquid on the mixing behaviour of systems consisting of large and small spheres [40, 41]. It was observed that as liquid was added, the tendency to segregate, which is well known for dry granulates [42, 43], was diminished. At a certain wetness, complete mixing occurred. In these experiments, the morphology of heaps formed by pouring mixtures of particles with two different sizes through an orifice was investigated.

In order to have a closer look at the observed effects, we have carried out experiments in which the agitation of the material is provided in a more homogeneous way, thus ensuring a more or less well defined granular temperature. Our technique of horizontally agitating the sample will be presented in detail below. Furthermore, the propensity of the system to segregate into large and small beads can be determined quantitatively in our set-up. We observed a strong impact of the liquid content upon the tendency of mixing or segregation, and a transition to a viscoplastic regime due to condensation of the grains into clusters, which was reported in [41], was clearly observed. However, the overall behaviour was found to be more complicated than previously reported, and we are able to explain all of the observed features within a rather simple model, based on hysteretic forces as described in the previous section. Most importantly, it turns out that the mixing behaviour can be used as a sensitive probe for the properties of the ensemble of the smaller particles.

A typical sample consisted of 150 ml of glass beads with $R = 2.5$ mm radius, sealed in a cylindrical jar (diameter 80 mm, cf figure 1) together with the same volume of smaller glass beads with radius r, which was varied from 50 to 500 μm, and a well defined amount of liquid. In order to prevent crystallization, the small beads were chosen to be slightly polydisperse: the spread in bead size ranged from 10 to 20%. The jars with the initially well mixed and homogeneously wetted grains were mounted on a shaker, with the cylinder axis upright. The shaking motion consisted of small horizontal circles with a diameter of 5 mm and a frequency of 20 revolutions per second, which corresponds to a velocity of the container walls of 0.38 m s^{-1}. When the segregation pattern did not change any more (typically after one half hour), photographs of the jars were taken and analysed. Two examples are shown in figure 16.

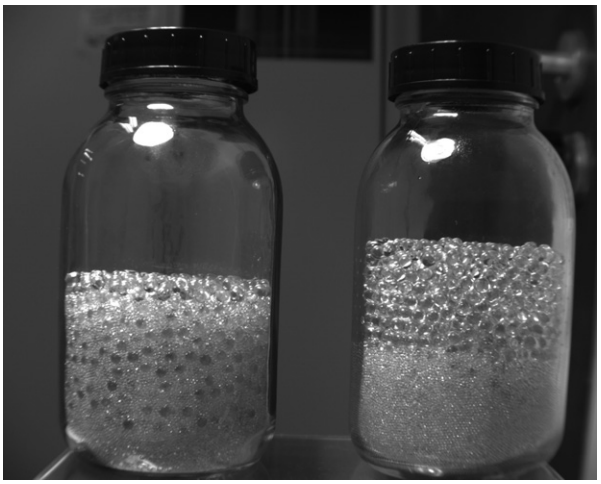

Figure 16. Horizontally shaken beads (with radii $R = 2.5$ mm and $r = 0.5$ mm) without water (left) and with the liquid content $w = 3 \times 10^{-4}$ (right). Both samples correspond to the gaseous regime (explained in the text) of the phase diagram (figure 3). At this radius r the increase of the segregation with increasing water content, which is characteristic for the gaseous regime, is particularly clear. The normalized height of the mixing zone was found to be 0.70 for the dry and 0.08 for the humid sample, respectively.

We defined the mixture zone as the zone in which both the smaller and the bigger particles were visibly present. This zone was observed to be rather homogeneous concerning the mixing ratio. Occasional analysis of horizontal slices of the samples revealed a small radial variation of the mixing ratio, which is not captured by the photographs, but the results given below are qualitatively valid for the whole volume. For the results presented here we used water as the liquid, but similar results were obtained using ethanol. We can therefore exclude that leaching of ions from the glass, and other side effects due to the specific properties of water, play a significant role [44]. The quantity we will discuss is the height of the mixture zone, divided by the total height of the sample, and is denoted by h. For perfect segregation, $h \to 0$, while $h = 1$ for perfect mixing. The amount of liquid added to the samples is denoted by the dimensionless quantity W, which is defined as the volume of the liquid divided by the total volume of the small beads (including the space between the beads).

In contrast to what one might anticipate on the basis of earlier work [40, 41], the propensity of mixing of the particles did not improve monotonically with the amount of liquid added. Instead, we found in most cases that the height of the mixture zone, h, was first *reduced* upon addition of water. Only after a certain amount of liquid had been added did the mixing improve. In figure 17, h is plotted as a function of W for two different r. The size of the large beads was kept constant. Clearly, there is a rather well defined liquid content above which the height of the mixing zone *increases* when more liquid is added.

The boundary between these two regimes (i.e., the minima of the curves as in figure 17) is indicated by the open squares in figure 18, which represents a phase diagram of the system in the plane spanned by the radius of the small beads, r, and the liquid content, W. The dotted line serves as a guide to the eye. The full circles correspond to the occurrence of complete mixing (i.e., $h = 1$). We can thus clearly distinguish three regimes, which we denote as *gaseous*, *intermediate*, and *viscoplastic* [45, 46], respectively. In what follows, we will discuss these regimes in some detail.

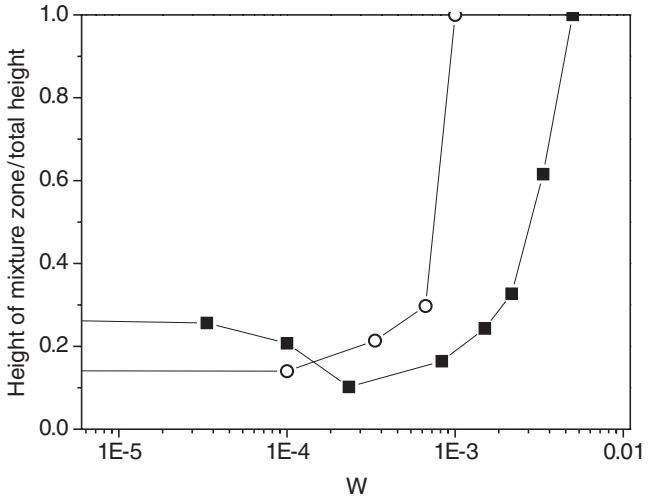

Figure 17. Normalized height of the mixture zone of shaken glass beads as a function of the amount of water added. The radius of the big beads was $R = 5$ mm; the diameter of the small beads was $r = 240$ μm (closed symbols) and $r = 140$ μm (open symbols), respectively.

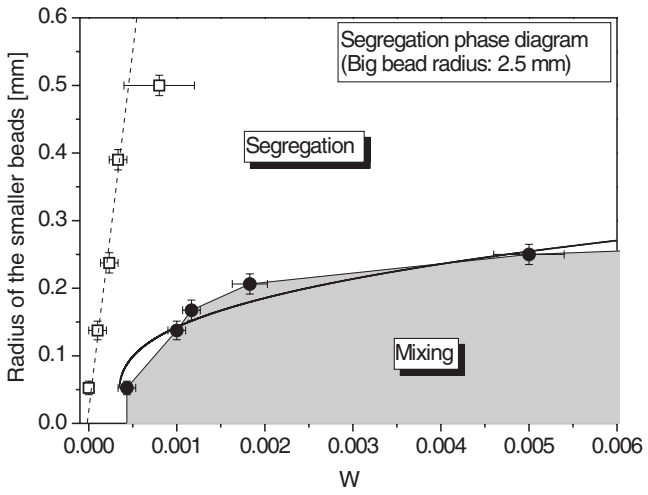

Figure 18. Segregation phase diagram in dependence on the liquid added. In the grey area there occurs no segregation, while in the white area segregation was observed. The steep dashed line separates the area in which the segregation increases by adding water (left) from the area in which the segregation decreases or stays the same (right). Note that $W_b \approx 0.0007$, as derived above.

Let us start with the transition to the *viscoplastic regime*, in which perfect mixing is observed. This transition, which occurs as $h \to 1$, appears quite abrupt when inspecting the experiment by eye. While the general motion of the whole sample was a kind of circular convection around the axis of the jar in the gaseous and intermediate regimes, the motion in the case of perfect mixing was reminiscent of kneading raisin dough. We identify this transition with the one reported recently by other authors [40, 41]. We assume that this transition into the viscoplastic regime occurs when the granular temperature of the system, i.e., the average

kinetic energy per bead, is no longer sufficient to break the liquid bridges between the beads, and is thus a kind of condensation within the granular gas, mediated by the liquid bridges.

In order to support this view, we have to discuss the involved forces in some detail. The force $F_B(d, w)$ exerted upon two adjacent beads by the liquid bridge has already been discussed above. The energy required to destroy such a bridge is given by

$$E_B(w) = 2\pi R\gamma f(w) \int_0^{d_r} g(d)\,\mathrm{d}d \tag{3}$$

where d_r is the distance at which the bridge pinches off. The integral can be well approximated as $w^{1/3}/3$ [36].

If we now equate the bridge energy, E_B, to the average kinetic energy of the small beads, $T := \frac{m}{2}\langle v^2\rangle$, we obtain, using the relation between W and w used in the previous sections, the implicit equation

$$R^2 - l\alpha^{1/3}W^{1/3}R + \frac{\delta^2}{\alpha W} = 0 \tag{4}$$

with $\alpha \approx 0.25$ (see above). Here we have introduced the characteristic length scale $l := \frac{\gamma}{\rho_g\langle v^2\rangle}$ (ρ_g is the mass density of the bead material. In our case, $\rho_g = 2500\ \mathrm{kg\,m^{-3}}$ (glass)). Equation (4) yields

$$R = \frac{l}{2}\alpha^{1/3}W^{1/3}\left(1 + \sqrt{1 - \left(\frac{W_c}{W}\right)^{5/3}}\right) \tag{5}$$

which intersects the W-axis at the critical moisture content $W_c = \frac{1}{\alpha}(2\delta/l)^{6/5}$, which only depends on the roughness amplitude, δ, and not on R. This function represents the phase boundary at which condensation sets in, and is indicated as the full curve in figure 18. From this best-fit curve we obtain $\delta \sim 500$ nm, as derived independently above. It is thus suggested that $W_c \approx W_b$, as corroborated by figure 18. From the fitted value of the intrinsic length scale l, and from the known density of the glass and the surface tension of the water, we get the average granular velocity, $v := \sqrt{\langle v^2\rangle} \approx 0.11\ \mathrm{m\,s^{-1}}$. This compares favourably with the velocity of the shaking motion, which is expected to be of the same order of magnitude.

Let us now turn to the *gaseous regime*. If there is no liquid in the sample at all, segregation is observed as usual, which has become known as the 'brazil nut effect' (BNE) [47–50]. As has been shown recently [43], this may be understood in a continuum picture, as follows. A granular medium is strongly dissipative due to the inelastic character of the impact kinetics of the grains, which is characterized by the restitution coefficient, ε. The latter is defined as the ratio of the particle velocities after and before impact, $\varepsilon = v'_{rel}/v_{rel}$. Thereby the granular temperature bath, which typically corresponds to thermal temperatures in the terakelvin range (see also the introduction), is internally coupled to the room-temperature bath provided by the atoms constituting the grains. This inherent state of non-equilibrium is the basic reason for the peculiar features of granular matter dynamics in general.

Now consider a spherical region with radius R within the granular gas. When a grain, or small bead, enters this region, it will have many impacts, and thereby lose a lot of energy, before it can leave this region again. When the latter is replaced by a solid sphere (i.e., a large bead of radius R), the grain will experience only one such impact. Consequently, the granular gas is hotter close to an intruder than far away in the bulk, because the intruder is a less effective heat sink. The granular gas is therefore also less dense around the intruder, and the latter rises due to the buoyancy of the 'bubble' of reduced density it carries around itself [43].

The height of the mixing zone is then a direct consequence of the balance between the hydrostatic pressure exerted by the large-bead fraction upon its lower interface, and the

buoyancy pressure exerted upon the same interface from below by the mixed phase. This picture is supported by the observation that the large beads acquire a rather uniform spacing within the mixed phase, which might then correspond to (twice) the thickness of the reduced density layer around each large bead [43].

The BNE increases as the energy loss upon impact is increased. This, however, is just what is achieved when liquid is added. The interparticle force exerted by the liquid has a hysteretic character [36, 51, 52], and is thus intrinsically dissipative. We thus expect the restitution coefficient to be reduced, and the BNE to become more prominent, when liquid is added. More precisely, the buoyancy of the reduced density bubbles around the large beads increases, and a shallower mixing zone is needed to balance the hydrostatic pressure of the large-bead column above it. Thus the height of the mixing zone is expected to decrease when liquid is added, which is what we observe. We thus assume that throughout this regime, which is defined by a monotonically decreasing height of the mixing zone, the physics of two-particle impact is affected by the liquid merely in the sense of a decrease in the restitution coefficient, ε.

7. Vertical agitation: fluidization by force

Another, more classical scheme of fluidization is to oscillate the container vertically. At sufficiently high amplitude and frequency, the grains start to move in an erratic fashion, very much reminiscent of the molecular motion in a liquid, while the density of the granulate remains close to dense packing. It is easy to derive conditions for this type of fluidization to occur. If the vertical position of the container is given by $A\cos(2\pi\nu t)$, its maximum acceleration is $4\pi^2 A\nu^2$. If this is less than the acceleration of gravity, it is clear that the granulate will remain at rest with respect to the container, and no fluidization takes place. If we define $\Gamma := 4\pi^2 A\nu^2/g$, also termed the Froude number, we can say that $\Gamma > 1$ is a necessary condition for fluidization. Experimentally, one finds that fluidization of dry granulates occurs at $\Gamma_{\mathrm{crit}} \approx 1.2$ [1, 53]. It manifests itself by the onset of an irregular, relative motion of the grains, usually accompanied by some convective flow within the container.

For the experiments to be described here, cylindrical glass containers with an inner diameter of 26 mm and a height of 40 mm were used. A container was filled with glass beads to a height of about 30 mm, with average radii ranging from 140 to 500 μm. In order to prevent crystallization, the beads in each sample were chosen to have a few per cent of polydispersity. Controlled amounts of liquid were added and the lid closed in order to prevent any loss of liquid by evaporation. For the results presented here, we used water as the liquid, but similar results were obtained using nonane. We can therefore exclude that leaching of ions from the glass, and other side effects due to the specific properties of water [44], play a significant role. The sample was agitated by hand for some minutes in order to obtain a homogeneous distribution of liquid. It was then was mounted onto an inductive shaker which could apply amplitudes between 1 μm and 1 mm, at frequencies between 20 and 333 Hz.

At fixed agitation frequency, the amplitude A was increased until a relative motion of the particles was visible through the glass wall. As figure 19 shows, the critical acceleration depended only weakly on frequency. In fact, for sufficiently high frequencies, it becomes independent of the latter [54]. In all cases, a certain hysteresis was observed, the upper branch of which we attribute to spurious cohesion within the pile, which is removed when fluidization occurs. The lower branch, observed upon reducing the amplitude, was found to be quite well defined and was taken henceforth for data acquisition.

As one expects, we found the critical acceleration for fluidization, Γ_{crit}, to depend strongly on the water content W, which is defined as the volume of liquid added, divided by the total sample volume. Complete saturation corresponds to $W \approx 0.36$, if the packing fraction of the

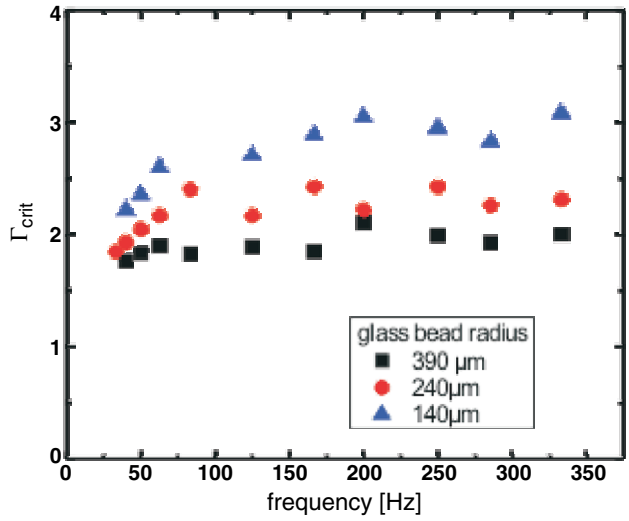

Figure 19. Dependence of the critical acceleration for fluidization on the frequency, for three different bead radii. The water content is 0.5%.

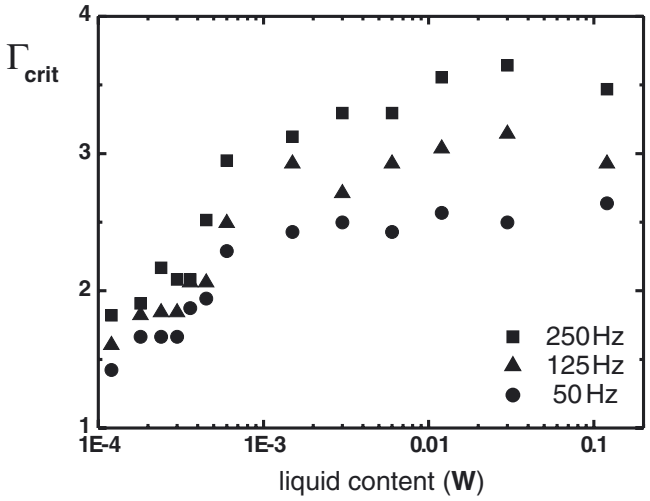

Figure 20. Dependence of the critical acceleration for fluidization on the water content, at three different frequencies for $R = 140\ \mu$m. Note the logarithmic scale.

beads is 64%. Figure 20 shows this for three different frequencies. We have found that in the high frequency limit all of our data can be well fitted with

$$\Gamma_{crit} = \Gamma_0 + f(W)\,p(R) \tag{6}$$

where R is the radius of the glass beads, $\Gamma_0 = 1.2$ is the critical acceleration for the dry case, and $f(0) = 0$. In other words, we find that the dependencies on moisture, bead size and frequency factorize, at least within the accuracy of our experiments. In what follows, we will discuss the functions $f(W)$ and $p(R)$.

Let us first turn to the dependence of Γ_{crit} on the liquid content. As figure 20 shows, Γ_{crit} first increases strongly from its 'dry' value ($\approx$1.2), but then stays roughly constant over about

two orders of magnitude in liquid content. This is strikingly reminiscent of the behaviour of the capillary force, F_B, between adjacent beads, as extensively discussed before. While we have used above the (heuristic) form given by equation (1), other forms are equally justified since they merely model the qualitative effect of the (poorly defined) roughness. We have found that we could fit our data well with

$$\Gamma_{crit} = \Gamma_0 + \Gamma_1 e^{-W_0/W}. \tag{7}$$

This result suggests that the extra acceleration required for fluidizing a wet bed of spherical beads seems to scale with the *force* of the capillary bridges between the beads. Although this might appear rather natural, it is in fact anything but trivial, since for the fluidization scheme in the preceding section we have found that it is the *binding energy* (or the energy required to break a bridge) which rules the fluidization parameters. This is not constant, but scales as $W^{1/3}$, in clear contrast to our data for Γ_{crit}. One may like to argue that since vertical agitation is a scheme based on acceleration the forces should be the paradigm quantities. These are linked to accelerations just by mass as a pre-factor. We will have to discuss which mass is the relevant one in our system.

It turned out that when Γ_0 was fitted anew for every sample the fit was not significantly better than with simply setting $\Gamma_0 = 1.2$ for all data sets. We thus kept this fixed value for the whole analysis. In this way we could extract, for all bead radii investigated, the quantity $\Gamma_1 = p(R)$, which corresponds to the extra acceleration required for fluidizing a bed of ideally spherical beads, without roughness.

In order to understand the dependence of Γ_1 on the bead radius, let us estimate the forces involved in the interaction of the container walls with the glass beads, and the acceleration force acting on the sample. The latter is given by

$$F_{acc} = (\Gamma - \Gamma_0)\rho_s V g \tag{8}$$

where $\rho_s = 1.60 \times 10^3$ kg m^{-3} is the weight density of the sample, and V is the sample volume considered. The capillary forces acting between the container walls and the glass beads are assumed to be similar to the force acting between two beads. The total capillary force is then

$$F_{cap} = 2\pi R\gamma \cos\theta \rho_{2D} O \tag{9}$$

where ρ_{2D} is the two-dimensional density of the bridges formed between the container wall and the glass beads, and O is the total surface considered. For hexagonal close packing, $\rho_{2D} = (2\sqrt{3}R^2)^{-1} \approx 0.29/R^2$. For our random packing, ρ_{2D} is certainly smaller than that, but of the same order of magnitude. Relative motion between the glass pile and the container walls will take place if $F_{acc} \geqslant F_{cap}$. The condition for the onset of fluidization is then

$$\Gamma_{crit} \approx \Gamma_0 + 0.29 \cos\theta \frac{2\pi\gamma}{\rho_s g} \frac{O}{VR}. \tag{10}$$

This predicts that the extra acceleration due to the addition of moisture, for ideal spheres and high frequency, will be inversely proportional to the bead radius. Figure 21 shows that this is well fulfilled. The solid line represents $p(R) = 254\ \mu\text{m}/R$. For a cylindrical sample with radius r, $V/O = r/2$. In our case, we thus have $O/V = 154$ m^{-1}. Furthermore, for water as the liquid, we have $\frac{2\pi\gamma}{\rho_s g} = 2.9 \times 10^{-5}$ m^2. Together with equation (10), this yields, for a closely packed surface layer, $0.29 \cos\theta = 0.057$, corresponding to a contact angle of about 75°. This is slightly different from earlier results [54], which may be due to our attention to the hysteresis in the transition, which we did not care so much about before. As mentioned above, the density of bridges at the container surface may be smaller than with close packing (i.e., the prefactor of the cosine being smaller than 0.29), yielding a smaller contact angle. In any case, the numbers we obtain appear quite reasonable.

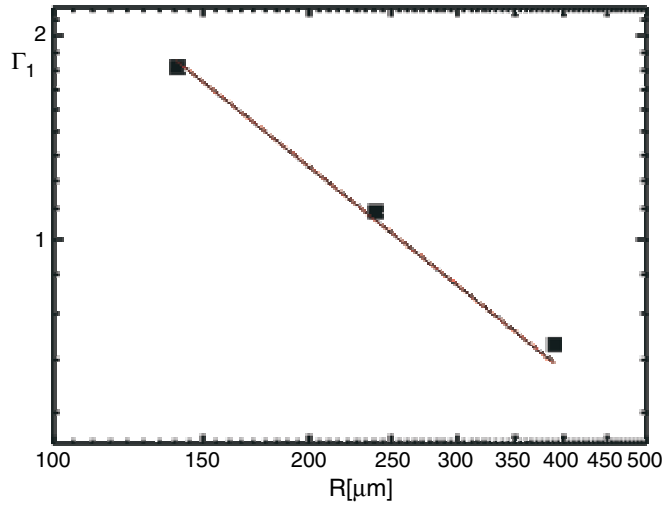

Figure 21. Dependence of the critical acceleration upon the radius of the glass beads. The solid line represents the theoretical model ($p(R) \propto 1/R$).

So far, our results suggest that fluidization of wet granular matter by vertical agitation, at least for our model system, can be quite well understood by the interaction of the pile with the walls of the container. If this is the case, the fluidization process must sensitively depend upon the capillary interaction of the glass beads with the walls of the container. We have tested this hypothesis by hydrophobizing the container walls. They were exposed to a solution of octadecyl trichlorosilane, which is well known to bind covalently to the glass surface. As a result, a monomolecular close packed layer of alcane forms on the glass, resulting in contact angles (with water) well above 100°. As our model suggests, the effect on the fluidization was dramatic: we were not able to reach fluidization with our apparatus, which was capable of applying accelerations up to $\Gamma \approx 20$!

A posteriori, our model appears quite natural, since in the vertical agitation scheme the relative motion of the container with respect to the sample does not necessarily imply a deformation of the pile, in contrast to horizontal agitation as discussed before. As a consequence, fluidization must start from the sample–container interface and must propagate inside. The bottom of the container exerts only a compressive motion and, since the sample itself is incompressible, is thus not capable of inducing any deformation at all. The cylindrical walls of the container cannot transfer kinetic energy, but can exert a shear force by means of the liquid bridges between the wall and the sample. Thus it appears justified to call this fluidization by force, as opposed to fluidization by energy as above.

Finally, let us consider the critical Froude number, Γ_{crit}, in the full range of liquid content, as we have done for the yield stress above. Data averaged over a wide range of frequencies are presented in figure 22. One clearly sees an abrupt change in Γ_{crit} around $W \approx 15\%$. This corresponds to the percolation threshold, above which there is one cluster of liquid which extends over the full sample. As a consequence, any acceleration Γ will lead to massive transport of liquid within the sample, and thus to transformations of bridge structures and, possibly, reorganization of the bridge network. It is straightforward to imagine that this leads to fluidization, even with $\Gamma \leqslant 1$. We thus can see that the fluidization behaviour is very sensitive to the global structure of the distribution of liquid within the sample. It may be left to further studies to investigate these effects in detail.

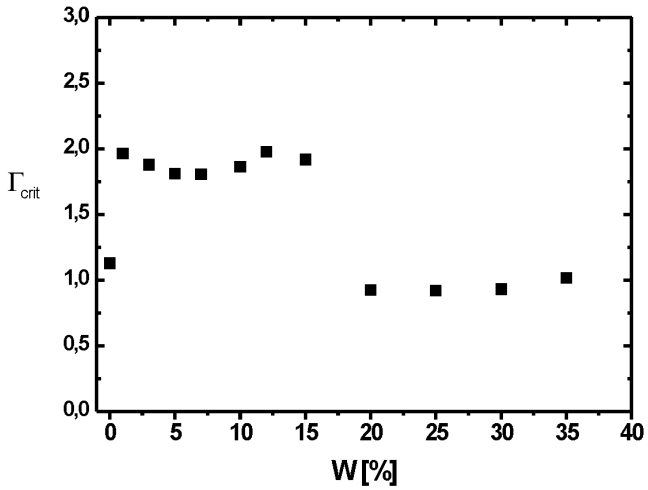

Figure 22. Critical acceleration amplitude for fluidization in a wider range of liquid content. At about 15% water content, a drastic change is observed, leading to fluidization significantly below $\Gamma = 1$.

8. Conclusions

We have described a rather simple model for the influence of liquid on the mechanical properties of granular material. Our experimental results support the idea that the network of capillary forces between the grains provides the stability of the wet granular pile, without friction being indispensable. It is clear that friction, and the shape of the grains in general, will alter the properties in their own fashion, but our results show that, in short, a sand castle can be built as well with frictionless, spherical grains. This picture is supported by our simulations as well as by our fluidization experiments, which can all be well explained assuming that the main physics is captured in a hysteretic attractive force, which acts between adjacent grains due to liquid capillary bridges.

Acknowledgments

Inspiring discussions with H Herrmann, S Luding, and S Linz are gratefully acknowledged. The authors thank the German Science Foundation for financial support within the priority programme 'Wetting and structure formation at interfaces'. MMK acknowledges the Alexander von Humboldt Foundation for generous funding.

References

[1] Ristow G H 2000 *Pattern Formation in Granular Materials* (Berlin: Springer)
[2] Jaeger H M, Nagel S R and Behringer R P 1996 *Rev. Mod. Phys.* **68** 1259
[3] Kadanoff L P 1999 *Rev. Mod. Phys.* **71** 435
[4] Clark W C and Mason G 1967 *Nature* **216** 826
[5] D'Anna G 2000 *Phys. Rev.* E **62** 982
[6] Ovarlez G, Kolb E and Clement E 2001 *Phys. Rev.* E **64** 060302(R)
[7] Forsyth A J, Hutton S and Rhodes M J 2002 *Powder Technol.* **126** 150
[8] Nasuno S, Kudrolli A, Bak A and Gollub J P 1998 *Phys. Rev.* E **58** 2161
[9] Cates M E, Wittmer J P, Bouchaud J-P and Claudin P 1998 *Phys. Rev. Lett.* **81** 1841

[10] Hartley R R and Behringer R P 2003 *Nature* **421** 928
[11] Mueggenburg N W, Jaeger H M and Nagel S R 2002 *Phys. Rev.* E **66** 031304
[12] Mikami T, Kamiya H and Horio M 1998 *Chem. Eng. Sci.* **53** 1927
[13] Israelachvili J N 1991 *Intermolecular and Surface Forces* 2nd edn (London: Academic)
[14] Hornbaker D J, Albert R, Albert I, Barabási A-L and Schiffer P 1997 *Nature* **387** 765
[15] Halsey T C and Levine A J 1998 *Phys. Rev. Lett.* **80** 3141
[16] Bocquet L, Charlaix E, Ciliberto S and Crassous J 1998 *Nature* **396** 24
[17] Fraysse N, Thomé H and Petit L 1999 *Eur. Phys. J.* B **11** 615
[18] Geromichalos D, Kohonen M M, Mugele F and Herminghaus S 2003 *Phys. Rev. Lett.* **90** 168702
[19] Mason G and Clark W 1968 *Nature* **219** 149
[20] Losert W, Bocquet L, Lubensky T C and Gollub J P 2000 *Phys. Rev. Lett.* **85** 1428
[21] Feng C and Yu A B 2000 *J. Colloid Interface Sci.* **231** 136
[22] Mason T G, Levine A J, Ertaş D and Halsey T C 1999 *Phys. Rev.* E **60** R5044
[23] Ganesan V and Brenner H 1998 *Phys. Rev. Lett.* **81** 578
[24] Lam C-H and Horváth V K 2000 *Phys. Rev. Lett.* **85** 1238
[25] Dubé M, Rost M, Elder K R, Alva M, Manjaniemi S and Ala-Nissila T 1999 *Phys. Rev. Lett.* **83** 1628
[26] Hernández-Machado A, Soriano J, Lacasta A M, Rodriguez M A, Ramirez-Piscina L and Ortin J 2001 *Europhys. Lett.* **55** 194
[27] Kardar M, Parisi G and Zhang Y-C 1986 *Phys. Rev. Lett.* **56** 889
[28] Geromichalos D, Mugele F and Herminghaus S 2002 *Phys. Rev. Lett.* **89** 104503
[29] Geromichalos D, Kohonen M M, Mugele F and Herminghaus S 2003 *Contact Angle, Wettability and Adhesion* (Zeist: VSP) p 385
[30] Stauffer D and Aharony A 1995 *Perkolationstheorie* (Weinheim: VCH)
[31] Simons S J R, Seville J P K and Adams M J 1993 *6th Int. Symp. on Agglomeration (Nagoya, Japan)* p 117
[32] Scott D 1960 *Nature* **188** 908
[33] Mason G 1968 *Nature* **217** 733
[34] Peters E A, Kollmann M, Barenbrug Th and Philipse A P 2001 *Phys. Rev.* E **63** 021404
[35] Jain N, Khakhar D V, Lueptow R M and Ottino J M 2001 *Phys. Rev. Lett.* **86** 3771
[36] Willet Ch D, Adams M J, Johnson S A and Seville J P K 2000 *Langmuir* **16** 9396
[37] Kohonen M M, Geromichalos D, Scheel M, Schier Ch and Herminghaus S 2004 *Physica* A **339** 7
[38] Da Cruz F, Chevoir F, Bonn D and Coussot P 2002 *Phys. Rev.* E **66** 051305
[39] Schulz M, Schulz B M and Herminghaus S 2003 *Phys. Rev.* E **67** 052301
[40] Samadani A and Kudrolli A 2000 *Phys. Rev. Lett.* **85** 5102
[41] Samadani A and Kudrolli A 2001 *Phys. Rev.* E **64** 051301
[42] Ottino J M and Khakhar D V 2000 *Annu. Rev. Fluid Mech.* **32** 55
[43] Trujillo L and Herrmann H J 2003 *Physica* A **330** 525
[44] Olivi-Tran N, Fraysse N, Girard P, Ramonda M and Chatain D 2002 *Eur. Phys. J.* B **25** 217
[45] Tegzes P, Albert R, Paskvan M, Barabasi A-L, Vicsek T and Schiffer P 1999 *Phys. Rev.* E **60** 5823
[46] Tegzes P, Vicsek T and Schiffer P 2002 *Phys. Rev.* E **89** 094301
[47] Williams J C 1976 *Powder Technol.* **15** 245
[48] Rosato A, Strandburg K J, Prinz F and Swendsen R H 1987 *Phys. Rev. Lett.* **58** 1038
[49] Knight J B, Jaeger H M and Nagel S R 1993 *Phys. Rev. Lett.* **70** 3728
[50] Möbius M E, Lauderdale B E, Nagel S R and Jaeger H M 2001 *Nature* **414** 270
[51] Crassous J, Charlaix E and Loubet J-L 1994 *Europhys. Lett.* **28** 37
[52] Zitzler L, Herminghaus S and Mugele F 2002 *Phys. Rev.* B **66** 155436
[53] Duran J 2000 *Sands, Powders, and Grains* (New York: Springer)
[54] Scheel M, Geromichalos D and Herminghaus S 2004 *J. Phys.: Condens. Matter* **16** S4213